

©2020. Licensed under the Creative Commons Attribution-NonCommercial-NoDerivatives 4.0 International <http://creativecommons.org/about/downloads>



Full version of can be found at: Wang, Yuwei, Zhang, Ziwei, Abo-zeid, Yasmin, Bear, Joseph C., Davies, Gemma-Louise, Lei, Xiaodong and Williams, Gareth R. (2020) SiO₂-coated layered gadolinium hydroxides for simultaneous drug delivery and magnetic resonance imaging. *Journal of Solid State Chemistry*, 286, p. 121291. <https://doi.org/10.1016/j.jssc.2020.121291>

SiO₂-coated layered gadolinium hydroxides for simultaneous drug delivery and magnetic resonance imaging

Yuwei Wang,^{a,b} Ziwei Zhang,^b Yasmin Abo-zeid,^c Joseph C. Bear,^d Gemma-Louise Davies,^e Xiaodong Lei,^a and Gareth R. Williams^{b*}

^a State Key Laboratory of Chemical Resource Engineering, Beijing University of Chemical Technology, P.O. Box 98, Beijing 100029, P. R. China

^b UCL School of Pharmacy, University College London, 29 – 39 Brunswick Square, London WC1N 1AX, UK

^c School of Pharmacy, Helwan University, Cairo, Egypt

^d Department of Chemical and Pharmaceutical Sciences, Kingston University, Penrhyn Rd, Kingston upon Thames, KT1 2EE

^e Department of Chemistry, University College London, 20 Gordon Street, London WC1H 0AJ, UK

* Author for correspondence. Email: g.williams@ucl.ac.uk; Tel: +44(0) 207 753 5868

Abstract

Layered gadolinium hydroxides (LGdH) have significant potential in simultaneous drug delivery and magnetic resonance imaging (MRI). In this work, we synthesized LGdH nanocomposites surface functionalised with SiO₂ nanodots (LGdH@SiO₂). We find these to have good dispersibility in cell culture medium, and a reduced tendency to aggregate compared to their uncoated analogue. Under the optimal reaction conditions, SiO₂ nanodots were evenly spread across the surface of the LGdH particles. We further intercalated ibuprofen (Ibu) and 5-fluorouracil (5FU) into LGdH@SiO₂, and explored the use of the resultant composites for drug delivery *in vitro*. While the SiO₂ coating could effectively reduce aggregation of the Ibu intercalate prepared by ion exchange from the parent LGdH, it was noted to increase aggregation in the case of the 5FU-loaded systems produced by coprecipitation. With a SiO₂ coating, 5FU release from the composite was almost zero-order at pH 7.4. The LGdH-5FU@SiO₂ composites can effectively inhibit the growth of A549 cells (a human adenocarcinoma cell line). In contrast, the Ibu-loaded materials are highly biocompatible. After SiO₂ modification, LGdH-5FU@SiO₂ retains the same proton relaxivity properties as LGdH-5FU, while LGdH-Ibu@SiO₂ becomes suitable for use as a negative contrast agent in MRI. Overall, we find the LGdH@SiO₂ nanocomposites are promising materials for theranostic applications.

1. Introduction

Layered materials have been widely employed in drug delivery.¹⁻³ Given that many APIs have carboxylic acid groups and can form anions, anion-exchanging layered systems have significant promise here. The latter are made up of positively charged layers held together by covalent bonding; anions are located between adjacent layers to ensure charge balance, and thereby a three-dimensional lamellar structure is constructed.⁴ Such anion-exchangeable layered materials not only have a rich interlayer chemistry, but can also be exfoliated into single layers.

Layered double hydroxides (LDHs) comprise the most frequently studied family of anion-

exchangeable layered materials⁵ and have been explored in diverse fields, for instance as flame retardants,^{6,7} catalysts and catalyst precursors,⁸ CO₂ adsorbents,⁹⁻¹³ cement additives,¹⁴ and drug delivery systems.¹⁵⁻¹⁸ Many LDHs have good biocompatibility and can provide pH sensitive payload release as well as protecting the anions in their interlayer regions.¹⁹⁻²² Their potency in drug delivery has been demonstrated in a number of studies.^{23,24} In addition, an increasing number of investigations into hierarchical LDH-drug nanocomposites with controllable morphology have been reported. For instance, Zhao *et al.* developed a method to obtain LDH@mesoporous silica core-shell nanomaterials with great potential for drug delivery and hyperthermia therapy.²⁵ In other work, Duan *et al.* designed three-component microspheres with a SiO₂-coated Fe₃O₄ core and a LDH shell, and showed that such materials can be used to purify recombinant proteins, as well as in drug delivery and as biosensors.²⁶

Beyond LDHs, there are alternative anion-exchangeable layered hydroxides that have been employed in drug delivery, albeit to a lesser extent. Layered rare earth hydroxides (LRHs) are one such group of such materials. The anion exchangeable class of LRHs can be defined as $[R_2(OH)_5]^+(A^{n-})_{1/n} \cdot yH_2O$ (where R represents lanthanide cations, Aⁿ⁻ is an anion, and 1 ≤ y ≤ 2), and includes materials such as $[Gd_2(OH)_5]Cl \cdot 1.5H_2O$ and $[Yb_2(OH)_5]Cl \cdot 1.5H_2O$. The inorganic anions in the interlayer region of LRHs can be replaced by alternative inorganic or bioactive organic molecules.^{27,28} Moreover, the presence of rare-earth ions in the layers gives LRHs magnetic and fluorescent features which cannot easily be obtained with LDHs. The twin benefits of anion-exchange and magnetic/fluorescent functionality give LRHs great potential for medical technologies.^{29,30} For instance, layered gadolinium hydroxides (LGdHs) can be applied in magnetic resonance imaging (MRI).²⁹ Xu *et al.* recently undertook a detailed investigation into the drug delivery and MRI performance of LGdH intercalates.³¹ They intercalated diclofenac, ibuprofen and naproxen into LGdH and found that the resultant LGdH-drug nanohybrids are promising materials for theranostic applications.

One major challenge to clinical translation arises from the fact the LRH and LDH nanoparticles can easily agglomerate in cell culture medium and *in vivo*, resulting in a smaller amount of nanosized particles that can be internalized by cells and thus reducing drug delivery efficiency.³² As a result of this aggregation, the nanocomposites often have low bioavailability and short circulation times *in vivo*. To prevent such aggregation, surface functionalization can be used.^{26,33-35} However, although a number of reports confirm the utility of LGdHs for MRI and/or drug delivery,^{30,31} to date there are no reports into the surface functionalization of LGdHs. This is a vital step which must be addressed for these materials to be translated towards clinical applications.

In this work, we explore for the first time the surface functionalization of LGdH systems. To do this we employ a silica-based coating, which has previously been found to be potent for LDH systems,³⁵ and report the synthesis of SiO₂ nanodot coated LGdH nanohybrids (LGdH@SiO₂). The cellular uptake of LGdH@SiO₂ was explored, before two model drugs (5-fluorouracil (5FU) and ibuprofen) were intercalated into the LGdH and LGdH@SiO₂ materials. These nanocomposites were fully characterized and their drug release profiles, biocompatibility and potential for magnetic resonance imaging studied in detail.

2. Experimental

2.1 Materials

Chemicals were purchased as follows: gadolinium chloride hexahydrate (Alfa Aesar, 99%), sodium

hydroxide (Fisher Scientific), sodium chloride (Sigma-Aldrich), *n*-octane (Alfa Aesar, >98%), L-arginine (Sigma-Aldrich, >98%), tetraethoxysilane (Alfa Aesar, 98%), Arsenazo III (Sigma-Aldrich), 5-fluorouracil (5FU; Fisher Scientific, 99%) and ibuprofen sodium salt (Ibu, Santa Cruz Biotechnology, >98%). All materials were used without further purification.

2.2 Synthesis

Preparation of LGdH and LGdH-5FU: The LGdH precursor was obtained using a hydrothermal method as previously reported.³¹ First, GdCl₃·6H₂O (2.23 g, 6 mmol) was dissolved in deionized water (15 mL). It was then added dropwise to a second solution containing NaCl (0.41 g, 7 mmol) and NaOH (0.42 g, 10.5 mmol) in deionized water (5 mL). After stirring for 10 min, the resultant suspension was transferred to a 23 mL Teflon-lined stainless steel autoclave and treated at 150 °C for 15 h. Solid products were collected by filtration, washed with deionized water and ethanol, and dried at 40 °C for 24 h. 5FU was intercalated into LGdH via co-precipitation. In brief, an aqueous solution (6 mL) of NaOH (0.2 g, 5 mmol) solution was added to a 0.4 M GdCl₃·6H₂O solution (7.5 mL) with stirring for 10 min. The slurry produced was separated after centrifugation and re-suspended in a solution (15 mL) containing 5FU (0.455 g, 3.5 mmol, pH=8-9, neutralized by 1 M NaOH solution). After stirring for 1 h at room temperature, the solid product was washed with deionized water and ethanol and then re-suspended in deionized water (20 mL). This suspension was transferred to a 23 mL Teflon-lined stainless steel autoclave and heated at 90 °C for 15 h.

Preparation of LGdH@SiO₂ and LGdH-5FU@SiO₂ nanocomposites: SiO₂ nanodots were coated on LGdH and LGdH-5FU following a previously reported procedure.³⁶ First, 0.42 mL of TEOS and 1.04 mL of octane were added to a deionized water solution of L-arginine (1 mg mL⁻¹, 14 mL). The mixture was stirred for 4 h at 60 °C.³⁷ A suspension of 56 mg of LGdH or LGdH-5FU in deionized water (14 mL) was then added into the above solution, and the reaction stirred at 60 °C for 20 h. The final nanocomposites were dried at 40 °C overnight after washing with deionized water and ethanol.

Preparation of LGdH-Ibu and LGdH-Ibu@SiO₂: LGdH-Ibu and LGdH-Ibu@SiO₂ were synthesized via an ion-exchange method using LGdH and LGdH@SiO₂ as precursors. 150 mg of the precursor material was dispersed in an aqueous solution (15 mL) containing ibuprofen sodium (222 mg, 0.1 mmol). After constant stirring at 60 °C for 24 h, the resultant materials were filtered, washed with deionized water and ethanol, and then dried in an oven at 40 °C overnight.

Preparation of LGdH-FITC and LGdH-FITC@SiO₂: Fluorescently-labelled systems were obtained by mixing a suspension of LGdH or LGdH@SiO₂ (6 mg mL⁻¹, 10 mL, in water) with an aqueous fluorescein isothiocyanate isomer I (FITC) solution (pH=10.0, 6 mg mL⁻¹, 10 mL). The mixtures were stirred at room temperature for 12 h, and the solid product isolated by filtration and washed repeatedly with water until the filtrate was colourless.

2.3 Characterization

X-ray diffraction: X-ray diffraction (XRD) data were collected in reflection mode on a Rigaku MiniFlex 600 diffractometer over the 2θ range from 3 to 45°, using Cu Kα radiation (λ = 1.5418 Å).

Infrared spectroscopy A Spectrum 100 spectrometer (PerkinElmer) fitted with an attenuated total reflectance attachment was employed to obtain spectra over the range 650 to 4000 cm⁻¹.

Elemental analysis: The content of Gd in the materials was analyzed using an ISA Jobin Yvon Ultima

2C inductively coupled plasma-optical emission (ICP-OES) simultaneous/sequential spectrometer running at 1 kW power with a 40.68 MHz radiofrequency Argon plasma. The plasma gas flow was 14 L min⁻¹. The nebuliser pressure was 2.6 bar at a 1 mL min⁻¹ sample flow rate. Spectral lines for gadolinium were measured at 326.224 nm. Samples were digested for ICP-OES using hot nitric acid.

Transmission electron microscopy (TEM) images were obtained on a CM 120 Bio-Twin instrument (Philips). For this, samples were first dispersed in ethanol, dropped onto carbon-coated TEM grids (TAAB), and then allowed to dry.

Dynamic light scattering (DLS) was undertaken to obtain the particle size distribution and zeta potential of the nanomaterials. 2 mg of sample was dispersed into 2 mL of water or 2 mL of a 10 mM NaCl solution for size and zeta potential measurements respectively. After ultrasonication for 20 min, data were collected on a Zetasizer NanoZS instrument (Malvern Instruments). Similar measurements were made where the nanocomposites were dispersed in DMEM medium with 10 % v/v FBS.

Stability assays were conducted under both acidic and neutral conditions. First, 0.2 mg of Arsenazo III was dissolved in 20 mL of HCl (pH 1.5) or phosphate buffered saline (PBS, pH 7.4). 20 mg of each of the LGdH materials was dispersed in the Arsenazo III solutions, and the mixture stirred at 37 °C for 2 h in acidic solution or 24 h in PBS. The suspension was then filtered through a PVDF-type syringe filter (0.22 µm) before a Cary 100 UV-visible spectrophotometer (Agilent Technologies) was employed to analyze the concentration of Gd³⁺ at 652 nm. For comparison, positive (GdCl₃·6H₂O) and negative controls (HCl or PBS) were established.

Drug release studies: PBS solutions at pH 5.0 and pH 7.4 were used as the release media. 30 mg of each sample was dispersed in 200 mL of the release medium under constant stirring at 100 rpm. The temperature was maintained at 37 ± 0.5 °C. At given time intervals, 5 mL of the solution was removed for analysis, and an equal volume of fresh pre-heated medium added to ensure a constant volume. The aliquots were filtered through a 0.22 µm filter and the drug concentration determined using a UV-vis spectrophotometer (7315, Jenway).

Cell culture: A549 cells, a adenocarcinomic human alveolar basal epithelial cell line, were used for *in vitro* studies. Cells were cultured in Dulbecco's modified Eagle's medium (DMEM; Gibco) supplemented with pre-heated fetal bovine serum (10% v/v), L-glutamine (1% v/v) and penicillin (1% v/v) in a humidified atmosphere (37 °C, 5% CO₂). For viability assays, A549 cells were pre-grown in 96 well plates. 1 × 10⁴ cells in 180 µL of medium were seeded into each well and cultured for 24 h. The medium was aspirated and 180 µL of DMEM containing various concentrations of LGdH-drug and LGdH-drug@SiO₂ nanocomposites was added. After a further 24 h incubation, the CellTiter-Glo™ assay was employed to investigate cell viability. The wells were aspirated, followed by addition of 100 µL of the fluorescent reagent and 100 µL of fresh medium to each well. The plate was then left for 10 min at room temperature. A SpectraMax M2e spectrophotometer was utilized to record luminescence data. The cell viability of the cells was determined using the following equation:

$$\text{Viability} = 100 \times \frac{(\text{Fluorescence of cells exposed to LGdH} - \text{background})}{(\text{Fluorescence of untreated cells} - \text{background})}$$

Three independent experiments were carried out, with three replicates per experiment. Data are reported as mean ± S.D.

Proton relaxivity: Samples were dispersed in an aqueous 1% w/v xanthan gum solution to obtain suspensions at various Gd³⁺ concentrations. These were added into NMR tubes of 10 mm diameter,

and homogeneous dispersions obtained after ultrasonication and microwave treatment. A Minispec mq20 relaxometer (23 MHz, 0.47T) was used to record both the longitudinal (T_1) and transverse (T_2) relaxation times at 37 °C. For the measurement of T_1 , the standard inversion-recovery method was employed with a typical 90° pulse calibration of 250 μ s with 4 scans per experiment; for T_2 , the Carr-Purcell-Meiboom-Gill (CPMG) method was used with 4 scans per experiment. A minimum of 3 different concentrations of stable nanoparticle samples were prepared and relaxation time measured for each sample. r_1 and r_2 relaxivity values were calculated from curves plotted of R_1 ($1/T_1, s^{-1}$) or R_2 ($1/T_2, s^{-1}$) vs. [Gd] concentration (mM) and analysis of the line of best fit for each sample. Gd concentrations of particles were obtained by ICP-OES as detailed above.

3. Results and discussion

3.1 Synthesis and characterisation of LGdH and LGdH@SiO₂

LGdH was synthesized following a previously reported protocol.³¹ TEM showed the LGdH nanoparticles to have plate-like morphologies and sizes of *ca.* 200 nm in width and 400 nm in length (Fig. 1a). DLS measurements concur with these values, giving a mean hydrodynamic diameter of 400 ± 10 nm (PDI 0.457). After mixing the LGdH-Cl material with tetraethoxysilane at a 1:1 mass ratio, the presence of spherical nanoparticles around 10-20 nm in size can be seen on the LGdH-Cl surface, indicating successful SiO₂ formation (Fig. 1b). Following purification, no free SiO₂ particles were evident on any of the grids examined, thus confirming that the SiO₂ is indeed surface grafted. After SiO₂ coating, the zeta potential of all the nanocomposites changed from $+56.8 \pm 2.5$ mV for LGdH to -33.1 ± 1.1 mV, consistent with the successful modification of particle surfaces with negatively charged SiO₂ nanodots.^{35,38} The DLS data reveal that the LGdH@SiO₂ particles have slightly smaller hydrodynamic diameters than the precursor, with Z-average particle sizes reduced (from 400 ± 10 nm) to 350 ± 8 nm (PDI 0.314). The reduction in PDI is consistent with reduced aggregation.

The XRD pattern of the LGdH precursor (Fig. 1c) matches well with the reported pattern³⁹ and the strong (010) basal lines indicate the successful formation of a layered structure. The IR spectrum (Fig. 1d) contains characteristic absorption peaks in the range from 3646 to 3383 cm^{-1} corresponding to the hydroxyl stretching vibrations, and a band at 1667 cm^{-1} which can be ascribed to the δ -bend of water.³¹ Other bands between 1600 and 1400 cm^{-1} result from the inclusion of small amounts of carbonate in the system. Elemental microanalysis data indicate the chemical formula of the LGdH material to be $[Gd_2(OH)_5]Cl_{0.8}(CO_3)_{0.1} \cdot H_2O$ (% obsd. [calcd.]: C 0.33 [0.26]; N 0 [0]; H 1.64 [1.56]). All these observations are in line with the literature³¹, confirming the successful synthesis of LGdH.

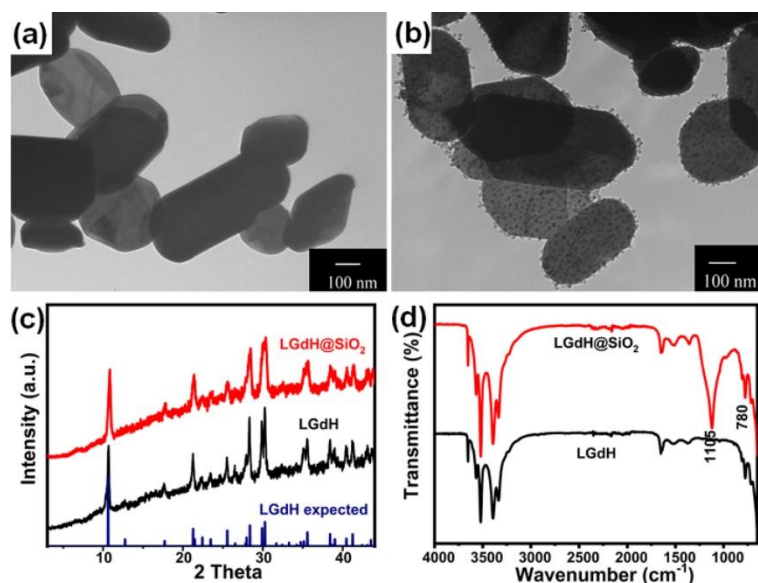


Fig. 1 Data demonstrating the successful synthesis of LGdH and LGdH@SiO₂. TEM images of (a) LGdH and (b) LGdH@SiO₂; (c) XRD patterns; (d) IR spectra.

XRD and IR data for the LGdH@SiO₂ system are given in Fig. 1c, d. The characteristic Bragg reflections of LGdH are retained in the XRD pattern after SiO₂ modification (Fig. 1c), and no changes except a slight broadening of the reflections (likely owing to the induction of some stacking defects) can be seen with LGdH@SiO₂. The growth of SiO₂ nanodots on the LGdH particle surface is further demonstrated in the FTIR spectra (Fig. 1d). In addition to the –OH and H₂O bands of LGdH, the LGdH@SiO₂ nanohybrids also exhibit two strong peaks at 1105 and 780 cm⁻¹, which can be attributed to Si-O-Si and O-Si-O stretching vibrations.⁴⁰ Hence, the LGdH precursor has been successfully functionalized with SiO₂ nanodots. When the size of the LGdH and LGdH@SiO₂ systems was studied in water and culture medium to explore the effect of protein absorption (which is inevitable *in vivo*) on particle behavior, the naked LGdH particles were observed to aggregate markedly, while the LGdH@SiO₂ particles appear stable (ESI, Fig. S1). The dispersibility and colloidal stability of LGdH in culture medium is thus improved after coating with SiO₂ nanodots.⁴¹

3.2 Drug intercalated LGdH and LGdH-drug@SiO₂ nanocomposites

We next explored the potential of using the LGdH@SiO₂ nanocomposite as a carrier to load Ibu (an anti-inflammatory drug) and 5FU (an anticancer drug). LGdH-Ibu and LGdH-Ibu@SiO₂ were prepared using ion exchange with pre-formed LGdH and LGdH@SiO₂. The reflections in XRD are broader and lower intensity after intercalation of Ibu, owing to the introduction of stacking defects, as has been noted many times in the literature.^{36,41} The characteristic reflections of LGdH-Ibu are also present in the LGdH-Ibu@SiO₂ system: both show a 010 reflection with the d-spacing of 23.58 Å. The interlayer spacing for the Ibu intercalate is close to that has been reported before (23.46 Å),³¹ and the XRD pattern for LGdH-Ibu (Fig. 2a) matches well with that from previous work.³¹

Successful intercalation of Ibu is further confirmed by IR spectroscopy (Fig. 2b). The broad peak at around 3500 cm⁻¹ can be ascribed to the OH stretching vibration of the hydroxide layers. In addition, peaks distinctive of Ibu at 1543 and 1400 cm⁻¹ (asymmetric and symmetric stretching vibrations of the –COO⁻ group)^{42,43} can be seen, verifying successful drug loading.³¹ Further, the two strong peaks at 2869 and 2955 cm⁻¹ are typical of alkyl stretching vibrations.⁴⁴ The LGdH-

drug@SiO₂ nanohybrid additionally displays a clear band at around 1105 cm⁻¹, confirming the coating with SiO₂. After the addition SiO₂, the intensity of the absorption bands at ca. 3500 and 1800 – 1400 cm⁻¹ are notably weaker, due to the presence of surface SiO₂.

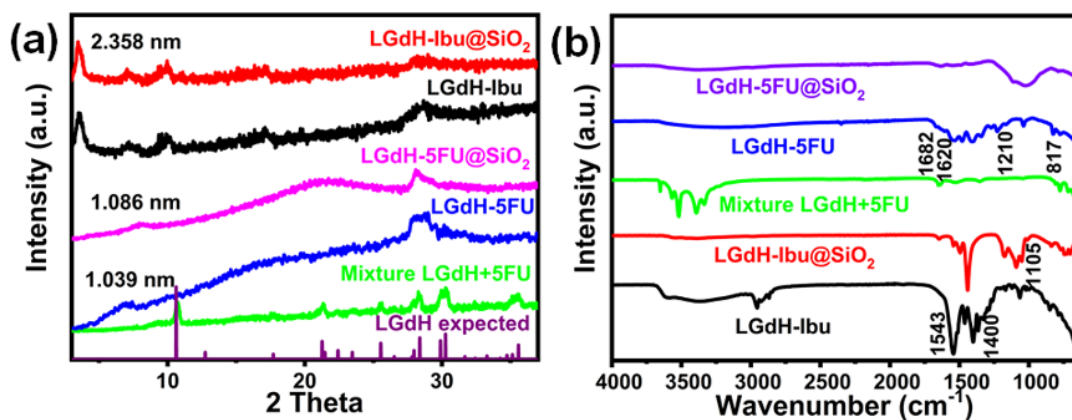


Fig. 2. (a) XRD patterns and (b) FTIR spectra for the LGdH-drug, and LGdH-drug@SiO₂ nanocomposites.

LGdH-5FU nanohybrids were synthesized for the first time in this work. The XRD data (Fig. 2a) show a broad 010 reflection at 10.39 Å for LGdH-5FU and at 10.86 Å for LGdH-5FU@SiO₂, an increase in *d*-spacing from the 8.41 Å of LGdH-Cl. This suggests intercalation of the drug, but the broadness of the reflections indicates materials with considerable structural disorder and makes it hard to confirm successful drug loading by XRD. To determine whether 5FU was intercalated or whether a physical mixture of the two had formed, the XRD pattern of a physical mixture of 5FU and LGdH was collected (Fig. 2a). The two patterns have distinct differences. The latter matches very closely the pattern of pure LGdH, indicating no intercalation. The stark differences between this and the pattern after coprecipitation suggests successful intercalation was achieved, since after co-precipitation the basal reflections of the parent LGdH are no longer visible. Further, the IR spectra of the physical mixture is similar to that of the LGdH precursor, while there are a range of additional peaks characteristic of 5FU in LGdH-5FU and LGdH-5FU@SiO₂. As shown in Fig. S2, these arise at 1682 and 1620 cm⁻¹ (C=O and C=C stretches), 1580-1300 and 817 cm⁻¹ (ring stretching modes),⁴⁵ and 1210 cm⁻¹ (C-F vibrations).⁴⁵ The IR results further confirmed the successful loading of 5FU into LGdH. As for the Ibu analogues, the drug and LGdH absorbance bands become weaker after functionalization with SiO₂.

CHN microanalysis was used to determine the elemental compositions of the drug intercalates (Table 1). The zeta potentials were additionally quantified (Table 1). The zeta potential of LGdH was +56.8 ± 2.5 mV, which reduces somewhat after intercalation with Ibu and 5FU (to +41.3 ± 0.9 and +30.6 ± 1.4 mV, respectively), indicative that there is some drug present on the surface of the particles. The zeta potential is further reduced after SiO₂ modification, to +6.4 ± 0.3 and -3.4 ± 5.8 mV. The drug loadings of LGdH-Ibu and LGdH-5FU (calculated from the elemental analysis findings) are 32.5 and 20.6 % w/w, respectively. In the SiO₂ coated systems, the loadings are 6.3 and 10.0 % w/w. The reduced loading in the case of LGdH-Ibu@SiO₂ (cf. LGdH-Ibu) is presumably a result of the SiO₂ nanospheres blocking entry to some of the interlayer edges, and thus impeding the ion exchange process. With the 5FU analogue, the reduction in loading after SiO₂ functionalisation is less significant, but nevertheless distinct; it must be the case that some 5FU leaked from the

composites during the surface modification step.

Fig. 3 gives TEM images of the drug-loaded nanocomposites. It can be observed that there were fewer nanodots on the surfaces of the drug-loaded systems compared with the LGdH@SiO₂ precursor, but the coating is nevertheless visible. The particle size of LGdH-5FU (36 ± 11 nm) measured by TEM is notably smaller than that of LGdH-ibu (405 ± 65 nm). This can be ascribed to the different synthetic routes which had to be applied. While the LGdH-Ibu@SiO₂ material appears to exist as isolated particles with large primary particles in TEM (Fig. 3a), the LGdH-5FU and LGdH-5FU@SiO₂ systems are more aggregated (Fig. 3b,c). These findings are borne out by the DLS data. We observe sizes of 673 ± 72 nm (PDI 0.41 ± 0.106) and 454 ± 16 nm (PDI 0.16 ± 0.04) for LGdH-Ibu and LGdH-Ibu@SiO₂ respectively, while for LGdH-5FU and LGdH-5FU@SiO₂ the equivalent values are 160 ± 5 nm (PDI 0.41 ± 0.04) and 1074 ± 69 nm (PDI 0.3 ± 0.03). It is thus clear that for the Ibu-loaded materials the SiO₂ coating causes a reduction in aggregation, as was noted for the parent LGdH. However, for the 5FU-loaded formulations the opposite trend is noted. This can presumably be attributed to the synthesis method: the Ibu was intercalated by ion exchange into the preformed LGdH layers, while 5FU-loaded systems had to be prepared by coprecipitation, resulting in notably smaller primary particle sizes. The increase in aggregation observed with LGdH-5FU@SiO₂ by DLS is also consistent with the zeta potential value of this material: the zeta potential is close to zero, which will encourage flocculation.

Table 1 The physicochemical properties of the LGdH-drug and LGdH-drug@SiO₂ nanocomposites. The zeta potential and size values are shown as mean ± SD (n = 3).

Sample	Zeta potential (mV)	Particle Size (nm)	Elemental contents (wt%)			Calculated chemical formula	Drug loading (wt%)
			obs. (Calc.)				
			C	N	H		
LGdH	56.8 ± 2.5	400 ± 10	0.33 (0.26)	–	1.64 (1.56)	[Gd ₂ (OH) ₅]Cl _{0.8} (CO ₃) _{0.1} ·H ₂ O	–
LGdH-5FU	41.3 ± 0.9	160 ± 5	8.12 (7.67)	3.88 (4.47)	1.44 (1.65)	[Gd ₂ (OH) ₅](C ₄ H ₂ FN ₂ O ₂) _{0.85} Cl _{0.15} ·H ₂ O	20.6
LGdH-5FU@SiO ₂	-3.4 ± 5.8	1074 ± 80	4.21 (3.73)	1.56 (2.18)	1.51 (1.32)	[Gd ₂ (OH) ₅](C ₄ H ₂ FN ₂ O ₂) _{0.47} Cl _{0.53} ·H ₂ O@1.8SiO ₂	10.0
LGdH-Ibu	30.6 ± 1.4	674 ± 80	25.84 (24.70)	–	3.32 (3.85)	[Gd ₂ (OH) ₅](C ₁₃ H ₁₇ O ₂) _{0.98} Cl _{0.02} ·H ₂ O	32.4
LGdH-Ibu@SiO ₂	6.4 ± 0.3	454 ± 16	4.91 (4.34)	–	2.09 (1.96)	[Gd ₂ (OH) ₅](C ₁₃ H ₁₇ O ₂) _{0.15} Cl _{0.85} ·H ₂ O@0.2SiO ₂	6.3

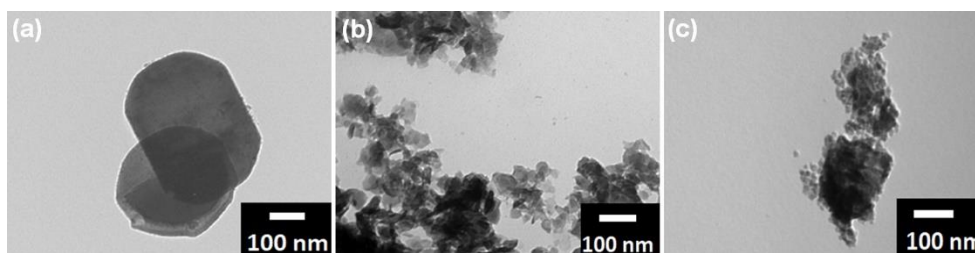


Fig. 3 TEM images of (a) LGdH-Ibu@SiO₂; (b) LGdH-5FU; and (c) LGdH-5FU@SiO₂.

3.3 Nanocomposite stability

Although Gd-based contrast agents are very powerful, and widely employed in the clinic, free Gd³⁺ is toxic to humans.⁴⁶ We thus employed the Arsenazo(III) assay to evaluate the stability of the nanocomposites at pH 1.5 (mimicking the stomach) and pH 7.4 (representing the general physiological environment).⁴⁷ Experiments were performed for 2 h and 24 h respectively, since these are approximately the amount of time that the composites would spend in the stomach and lower intestinal tract *in vivo* following oral application. Arsenazo(III) coordinates with Gd³⁺ to obtain a strongly-bound complex with a pH-dependent λ_{\max} .⁴⁸ It has been reported that the λ_{\max} of the complex is 650 nm when the pH lies in the range of 3-4 or 6.4-8.⁴⁹⁻⁵¹ The results of assays in which the nanoparticles were incubated in different pH solutions are presented in Fig. 7.

In both acidic and neutral solutions, the positive control (GdCl₃) displays a strong peak at 652 nm, suggesting the formation of the Gd³⁺-Arsenazo complex. HCl or PBS alone has minimal absorbance at this wavelength. At pH 1.5, the LGdH, LGdH@SiO₂, LGdH-drug and LGdH-drug@SiO₂ systems all show similar absorbance to the positive control at 652 nm, indicating that free Gd³⁺ has been released from the samples. Concentrations of 174 – 208 $\mu\text{g}/\text{mL}$ are observed (see Fig. S3 for the calibration plot), indicating that 27.3% (LGdH), 19.2% (LGdH@SiO₂), 29.5% (LGdH-Ibu), 23.1% (LGdH-Ibu@SiO₂), 40.1% (LGdH-5FU) and 32.3% (LGdH-5FU@SiO₂) of the Gd³⁺ had been released after 2 h. The Gd leaching is reduced after the introduction of SiO₂. In contrast, at pH 7.4 the LGdH and LGdH-Ibu nanocomposites show only minimal absorbance at 652 nm, equating to 7.0 and 7.6% of the Gd content leaching, respectively. However, there is still significant absorbance visible for the 5FU systems at this pH, indicating a lack of stability. The Gd leaching is reduced after surface coating with SiO₂ for 5FU (from 15.1% to 9.2%).

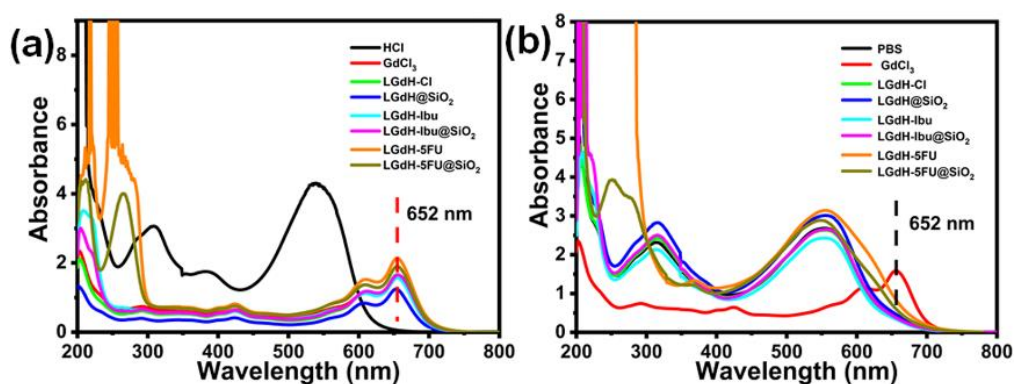


Fig. 4 Assays of the stability of the various nanocomposites at (a) pH 1.5 for 2 h, and (b) pH 7.4 for 24 h, employing the Arsenazo(III) method.

3.4 Drug release

Drug release from the LGdH-drug and LGdH-drug@SiO₂ composites were explored at pH 5 and pH 7.4. The pH 5 release medium was selected to mimic a late endosomal/lysosomal environment, while the pH 7.4 solution represents normal physiological conditions. The former was chosen because it is generally believed that the cellular uptake of small particles (< 200-300 nm) involves endocytosis in most cases, while larger particles were found to be taken up by phagocytosis.⁵²⁻⁵⁵ Drug release data are given in Fig. 5. A burst of release is seen in most cases, which presumably can be attributed to the drug at the particle surface. LGdH-5FU exhibits similar drug release rates at both pH 5 and pH 7.4. LGdH-5FU@SiO₂ displays a reduced final release percentage (around 45% at both pH 7.4 and pH 5) than LGdH-5FU after 48 h, which is likely due to the surface coating providing a steric barrier to drug release. At pH 7.4, the LGdH-5FU@SiO₂ system released the drug in a zero-order manner in the first 25 h, while it behaves more similarly to LGdH-5FU at pH 5.

For LGdH-Ibu, the final release percentage reaches almost 100 % after 48 h, in all the media studied (Fig. 5). Ibu release from LGdH-Ibu reached 50 % after 180 min at pH 7.4, while it takes longer (about 670 min) to reach 50 % release at pH 5. Ibu is a pH-sensitive drug with lower solubility in acidic conditions, which is likely to be responsible for the difference in release rates.⁵⁶ For the LGdH-Ibu@SiO₂ system, the amount of drug released is notably less than that of LGdH-Ibu after 48 h (41% at pH 7.4, 30% at pH 5). Moreover, this material releases more rapidly in the earlier stages of the experiment, arriving at a maximum value after 3-5 h. It also appears that after reaching this maximum there is a small decline in drug release, likely to be due to some drug adsorbing back onto the LGdH composite.

The SiO₂ coating reduces the amount of drug released for both Ibu and 5FU, thought to be because the SiO₂ nanodots on the surface of the particles provide some steric hindrance to drug release. Greater release percentages are observed for LGdH-Ibu than LGdH-5FU at the end of the experiment, which is expected to be a result of the ionisation of the Ibu COOH group increasing its solubility at the pHs investigated (in contrast, 5FU will form a neutral molecule after release).^{57,58}

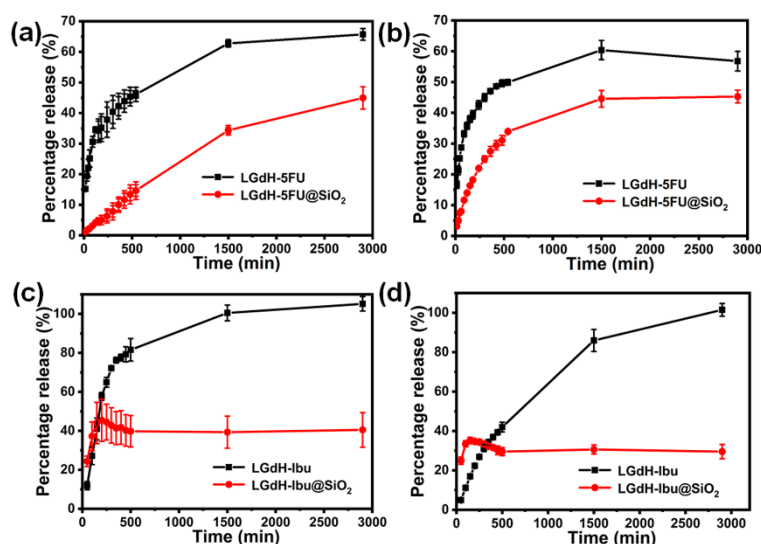


Fig. 5 Drug release for 5FU at (a) pH 7.4, (b) pH 5, and Ibu at (c) pH 7.4, (d) pH 5. Three independent experiments were performed, and data are shown as mean \pm S.D.

The Bhaskar (Eqn. 1) and Avrami-Erofe'ev models (Eqn. 2) were utilized to fit the release data.

$$\ln\left(1 - \frac{M_t}{M_{inf}}\right) = kt^{0.65} \quad (1)$$

$$\ln(-\ln(1 - \alpha)) = n \ln k + n \ln t \quad (2)$$

For eqn (1), M_t is the amount of drug released at time t , and M_{inf} the total amount of drug loaded in the carrier. For eqn (2), $\alpha = M_t / M_{inf}$, n is an exponent that provides information on the reaction mechanism, and k is a rate constant.

Fits of the two models to the release data are shown in the ESI, Figs. S4 and S5. For LGdH-5FU, LGdH-5FU@SiO₂ and LGdH-Ibu both models in general fit the data well in both pH environments, although the Bhaskar fits for LGdH-5FU@SiO₂ at pH 7.4 and for LGdH-5FU at pH 7.4 and 5 are rather poor. For LGdH-Ibu@SiO₂, the release data cannot be fitted satisfactorily with either model. The Bhaskar model assumes that diffusion of the drug ions and/or replacement anions through the particle limits the release rate, and thus for LGdH-Ibu this can be assumed to be the rate limiting step to release.^{59,60} The value of n in Avrami-Erofe'ev equation also provides some information on the reaction mechanism.⁶¹ The values of n for LGdH-5FU@SiO₂ in the pH 7.4 and pH 5 solutions were 0.74 and 0.72, while those for LGdH-5FU were 0.37 and 0.38. All of these suggest diffusion control, indicating that diffusion of replacement ions through solution limits the rate. This is consistent with the poor Bhaskar fit for these systems.⁶² For LGdH-Ibu, the values of n were closer to 1.0, indicating a 2D nucleation-controlled process. This is in agreement with the much better Bhaskar fit for this material. However, it should be noted that there a range of potential interpretations of the n values obtained, and thus it is not possible to draw definitive conclusions here.

3.5 Cell viability

The cytotoxicity of the LGdH and LGdH@SiO₂ nanohybrids to A549 cells after 24 h was explored at a range of concentrations (Fig. 6a). The cell viability is always more than 100% of the untreated cells control, indicating that the nanocomposites are biocompatible and do not induce cytotoxicity to A549 cells.

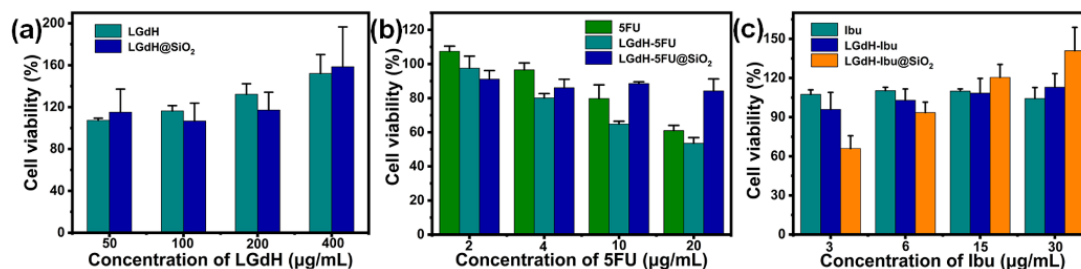


Fig. 6. *In vitro* cytotoxicity data for (a) LGdH and LGdH@SiO₂; (b) 5FU intercalates; and, (c) Ibu intercalates. The concentration values given for 5FU and Ibu are those which would arise if 100% of the intercalated drug was released from the composite.

It is clear from the data in Fig. 6 that the 5FU formulations are toxic to the cells, while the Ibu materials in general are not. The LGdH-Ibu@SiO₂ system does appear to be toxic at low concentrations, however. The reasons for this are not clear. In most cases, the SiO₂-functionalised

materials result in higher viability than those without the surface coating.

These results can be explained by considering a balance of drug release and cellular uptake. In the 5FU case, the extent of release at the 24 h timepoint is reduced after SiO₂ coating (from 62.8% to 34.4% after SiO₂ coating). Both nanocomposites display more effective inhibition of cancer cell growth than free 5FU when the concentration of 5FU is 4.28 µg/mL or below. When the concentration increased to 10.7 and 21.4 µg/mL, more cancer cells are killed by LGdH-5FU than free 5FU, while LGdH-5FU@SiO₂ is less potent. All the materials loaded with Ibu exhibit high biocompatibility, and seem to encourage cell growth. This is consistent with a previous study in the literature using Caco-2 cells.³¹

3.6 Magnetic resonance imaging (MRI) behaviour

MRI contrast agents (CAs) are regularly used clinically to improve image resolution and aid in disease diagnosis.⁶³ The use of Gd-based nanomaterials as so-called positive MRI CAs has been widely explored.⁶⁴⁻⁶⁶ Such materials boost signal contrast through decreasing indigenous water proton relaxation times through close molecular interactions, as described by Solomon, Bloembergen and Morgan equations.^{67,68} The efficacy of MRI contrast agents can be assessed through the measurement of proton relaxation rates. The relaxation rate of water protons with respect to the concentration of contrast agent (according to Equation 1) provides an agents' relaxivity ($r_{1,2}$ in mM⁻¹s⁻¹), which allows quantitative comparison between different CA species.

$$r_{1,2} = \frac{R_{1,2,obs} - R_{1,2,sol}}{[CA]} \quad (3)$$

Where $R_{1,2,obs}$ is the observed relaxation rate of the agent in aqueous suspension (where $R_1=1/T_1$ and T_1 is the longitudinal relaxation time of water protons and $R_2=1/T_2$ and T_2 is the transverse relaxation time of water protons), $R_{1,2,sol}$ is the relaxation rate of the unaltered solvent system (*i.e.* in the absence of contrast agent) and $[CA]$ is the mM concentration of the contrast agent in suspension, in this case, the $[Gd]$ as measured by ICP-OES. In order to assess the contrast agent behaviour of LGdH-drug and LGdH-drug@SiO₂, proton relaxation was measured at 23 MHz and 37 °C. r_1 relaxivity is dominated by an inner sphere mechanism (of water coordination and exchange with paramagnetic Gd species). Herein, LGdH composites may be expected to exhibit r_1 relaxation enhancement, due to the presence of Gd₂(OH)₅⁺ within their structures, with nearby hydrogen bonded water facilitating coordinative water exchange. The parent LGdH materials exhibit an r_1 relaxivity of 3.27 mM⁻¹s⁻¹ (Fig. 7), which is comparable with molecular Gd chelate species and lower than other nanostructured Gd-species in literature, which may imply that water exchange is slow within these compositions. The parent LGdH materials show a decrease in r_1 relaxivity upon intercalation with drug moieties ($r_1=2.02$ mM⁻¹s⁻¹ for LGdH-Ibu and $r_1=1.51$ mM⁻¹s⁻¹ LGdH-5FU), which is likely due to decreased water coordination and exchange due to the presence of the drug species in the internal cavities of the composites. The difference in r_1 values between LGdH-Ibu and LGdH-5FU are due to the large differences in composite size, as previously described (in section 3.2). Upon modification with SiO₂ nanodots, r_1 values for both composites reduced further ($r_1=0.81$ mM⁻¹s⁻¹ for LGdH-Ibu@SiO₂ and $r_1=0.41$ mM⁻¹s⁻¹ LGdH-5FU@SiO₂), with SiO₂ reducing the ability for water to coordinate and exchange with internalised Gd species on the composites due to their external location blocking water access.

r_2 relaxivity is dominated by outer sphere mechanisms and results from diffusive water interaction with inhomogeneities in local magnetic field strengths generated by magnetic

composites. Herein, r_2 values are significantly higher than those observed for r_1 ($r_2=27.26 \text{ mM}^{-1}\text{s}^{-1}$ for LGdH). High r_2 relaxivities have previously been reported for LGdH species⁶⁹ and here, r_2 relaxivities follow a similar trend to that observed for r_1 . LGdH-5FU samples exhibited lower r_2 values ($r_2=1.94 \text{ mM}^{-1}\text{s}^{-1}$ for LGdH-5FU and $r_2=0.81 \text{ mM}^{-1}\text{s}^{-1}$ LGdH-5FU@SiO₂), due to their smaller particle sizes. An exception is observed for LGdH-Ibu@SiO₂ ($9.78 \text{ mM}^{-1}\text{s}^{-1}$), whose r_2 increased relative to LGdH-Ibu ($4.36 \text{ mM}^{-1}\text{s}^{-1}$). This may be due to the presence of SiO₂ trapping water molecules inside internal LGdH cavities; alongside Ibu, this could enhance r_2 values due to close proximity with the Gd species providing enhanced second sphere effects.

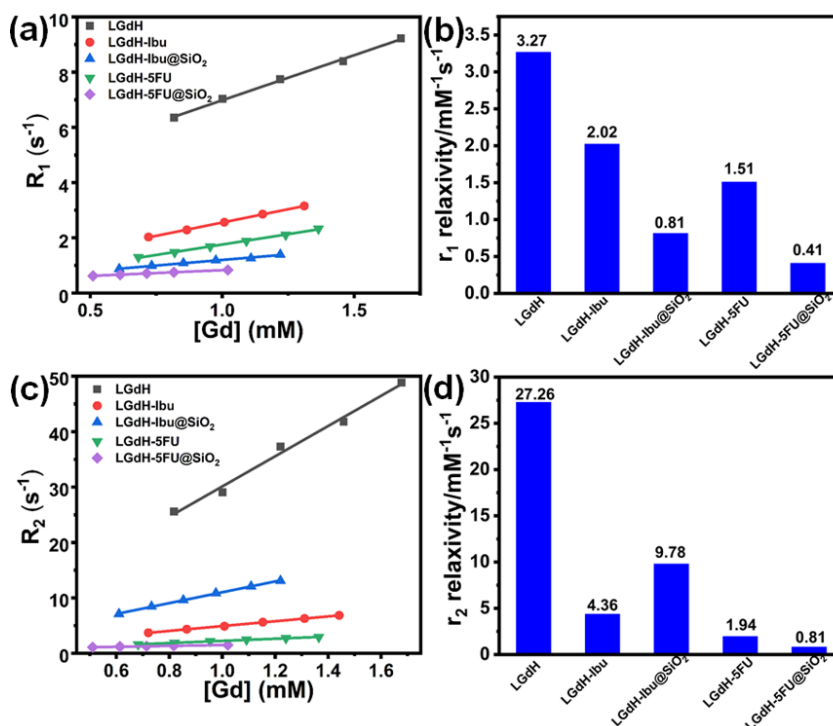


Fig. 7. Relaxivity data for the LGdH, LGdH-drug and LGdH-drug@SiO₂ nanocomposites, displaying (a and b) r_1 and (c and d) r_2 plots; and corresponding relaxivity (unit: mM⁻¹s⁻¹).

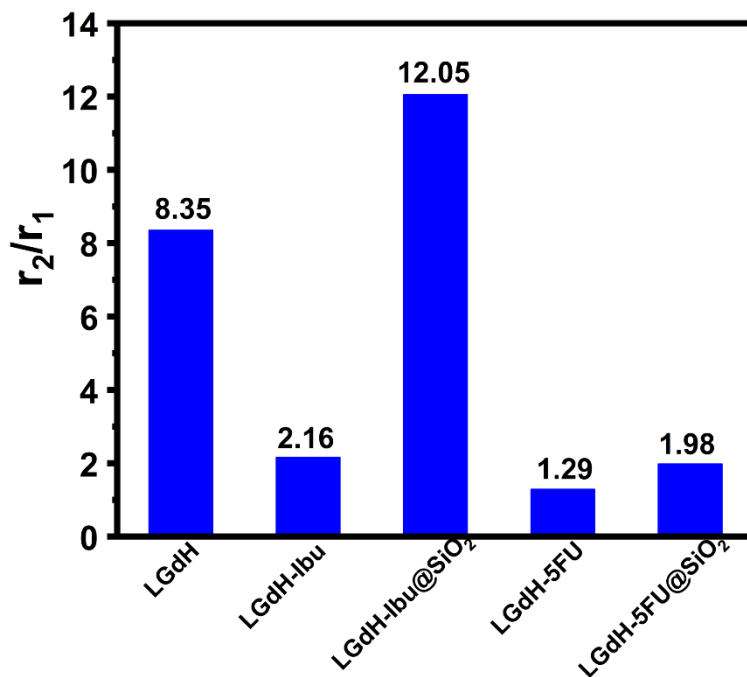


Fig. 8. The r_2/r_1 values for the nanocomposites.

In general, MRI CAs can be classified as ‘positive’ CAs (exhibiting areas of hyperintense signal) or ‘negative’ CAs (exhibiting hypointense signal), depending on their r_2/r_1 ratio, with positive CAs possessing r_2/r_1 values of ~ 1 , and negative CAs presenting values $r_2/r_1 \gg 1$.⁷⁰ Herein, r_2/r_1 values for LGdH, LGdH-Ibu, LGdH-Ibu@SiO₂, LGdH-5FU and LGdH-5FU@SiO₂ are 8.35, 2.16, 12.05, 1.29 and 1.98, respectively (Fig. 8), indicating that the parent LGdH and Ibu loaded nanocomposites exhibit preferentially ‘negative’ contrast enhancement capabilities, due to their large particle sizes and intercalation with Ibu, which enhances outer sphere interactions. LGdH-5FU and LGdH-5FU@SiO₂ on the other hand, appear to show much lower overall relaxivity enhancements, and as such, the r_2/r_1 ratio as an assessment of class of contrast agent becomes unreliable.

4. Conclusions

In this work, SiO₂ coated layered Gd hydroxide (LGdH) nanocomposites were generated and explored as potential theranostic agents. The SiO₂ coating method was first optimised, after which particles with good dispersibility were obtained via a facile and reproducible method. SiO₂ nanodots were uniformly distributed across the surface of LGdH nanoparticles under the optimal synthetic conditions. The coating reduced the particle size and helped to reduce particle aggregation. Ibuprofen (Ibu) and 5-fluorouracil (5FU) were further intercalated into the LGdH and LGdH@SiO₂ nanocomposites. While the SiO₂ coating could effectively reduce aggregation of the Ibu intercalate generated by ion exchange from the parent LGdH, it was noted to increase aggregation in the case of the 5FU-loaded systems prepared by coprecipitation. The drug release profile is pH-sensitive in the case of the ibuprofen composites, and was profoundly affected by the SiO₂ coating. In particular, LGdH-5FU@SiO₂ showed zero-order release at pH 7.4, and is more toxic to cancerous cells than free 5FU at higher concentrations. In contrast, the ibuprofen analogue is highly biocompatible. LGdH nanocomposites demonstrated strong r_2 relaxivity enhancement and LGdH-Ibu samples in particular demonstrated promise as negative contrast agents.

Acknowledgements

The authors would like to thank the China Scholarship Council for awarding Y.W. a scholarship to study at UCL, and the British Council and Science and Technology Development Fund in Egypt for awarding a Newton-Mosharafa Researcher Links Travel Grant to Y.A.-z. We are also grateful to Andrew Weston (UCL School of Pharmacy) for TEM data.

References

1. J. M. Oh, M. Park, S. T. Kim, J. Y. Jung, Y. G. Kang and J. H. Choy, *Journal of Physics and Chemistry of Solids*, 2006, **67**, 1024-1027.
2. L. Wang, H. Xing, S. Zhang, Q. Ren, L. Pan, K. Zhang, W. Bu, X. Zheng, L. Zhou, W. Peng, Y. Hua and J. Shi, *Biomaterials*, 2013, **34**, 3390-3401.
3. G. Huang, K. L. Zhang, S. Chen, S. H. Li, L. L. Wang, L. P. Wang, R. Liu, J. Gao and H.-H. Yang, *Journal of Materials Chemistry B*, 2017, **5**, 3629-3633.
4. F. Geng, R. Ma and T. Sasaki, *Accounts of Chemical Research*, 2010, **43**, 1177-1185.
5. Q. Wang and D. O'Hare, *Chemical Reviews*, 2012, **112**, 4124-4155.
6. C. Nyambo, P. Songtipya, E. Manias, M. M. Jimenezgasco and C. A. Wilkie, *Journal of Materials Chemistry*, 2008, **18**, 4827-4838.
7. C. Manzi Nshuti, D. Wang, J. M. Hossenlopp and C. A. Wilkie, *Journal of Materials Chemistry*, 2008, **18**, 3091-3102.
8. X. Xu, R. Lu, X. Zhao, S. Xu, X. Lei, F. Zhang and D. G. Evans, *Applied Catalysis B Environmental*, 2011, **102**, 147-156.
9. Q. Wang, J. Luo, Z. Zhong and A. Borgna, *Energy & Environmental Science*, 2010, **4**, 42-55.
10. Q. Wang, H. H. Tay, D. J. Wei, L. Chen, Y. Liu, J. Chang, Z. Zhong, J. Luo and A. Borgna, *Chemosuschem*, 2010, **3**, 965-973.
11. Q. Wang, Z. Wu, H. H. Tay, L. Chen, Y. Liu, J. Chang, Z. Zhong, J. Luo and A. Borgna, *Catalysis Today*, 2011, **164**, 198-203.
12. Q. Wang, H. T. Hui, Z. Guo, L. Chen, Y. Liu, J. Chang, Z. Zhong, J. Luo and A. Borgna, *Applied Clay Science*, 2012, **55**, 18-26.
13. Q. Song, W. Liu, C. D. Bohn, R. N. Harper, E. Sivaniah, S. A. Scott and J. S. Dennis, *Energy & Environmental Science*, 2012, **6**, 288-298.
14. J. Plank, Z. Dai, H. Keller, F. V. Hössle and W. Seidl, *Cement & Concrete Research*, 2010, **40**, 45-57.
15. A. C. S. Alcântara, P. Aranda, M. Darder and E. Ruiz-Hitzky, *Journal of Materials Chemistry*, 2010, **20**, 9495.
16. V. Rives, M. Del Arco and C. Martín, *Journal of Controlled Release*, 2013, **169**, 28-39.
17. L. Li, W. Gu, J. Chen, W. Chen and Z. P. Xu, *Biomaterials*, 2014, **35**, 3331-3339.
18. V. Rives, M. del Arco and C. Martín, *Applied clay science*, 2014, **88**, 239-269.
19. S. Zhang, Z. Chu, C. Yin, C. Zhang, G. Lin and Q. Li, *Journal of the American Chemical Society*, 2013, **135**, 5709-5716.
20. S. J. Choi, G. E. Choi, J. M. Oh, Y. J. Oh, M. C. Park and J. H. Choy, *Journal of Materials Chemistry*, 2010, **20**, 9463-9469.
21. M. Chakraborty, S. Dasgupta, S. Sengupta, J. Chakraborty, S. Ghosh, J. Ghosh, M. K. Mitra, A. Mishra, T. K. Mandal and D. Basu, *Ceramics International*, 2012, **38**, 941-949.
22. D. Pan, H. Zhang, T. Fan, J. Chen and X. Duan, *Chemical Communications*, 2011, **47**, 908-910.

23. A. Hakeem, G. Zhan, Q. Xu, T. Yong, X. Yang and L. Gan, *Journal of Materials Chemistry B*, 2018, **6**, 5768-5774.
24. M. Yasaei, M. Khakbiz, E. Ghasemi and A. Zamanian, *Applied Surface Science*, 2019, **467-468**, 782-791.
25. H. Bao, J. Yang, Y. Huang, Z. P. Xu, N. Hao, Z. Wu, G. Q. M. Lu and D. Zhao, *Nanoscale*, 2011, **3**, 4069-4073.
26. M. Shao, F. Ning, J. Zhao, M. Wei, D. G. Evans and X. Duan, *Journal of the American Chemical Society*, 2012, **134**, 1071-1077.
27. W. Li, Q. Gu, F. Su, Y. Sun, G. Sun, S. Ma and X. Yang, *Inorganic chemistry*, 2013, **52**, 14010-14017.
28. Q. Gu, Y. Sun, N. Chu, S. Ma, Z. Jia and X. Yang, *European Journal of Inorganic Chemistry*, 2012, **2012**, 4407-4412.
29. B. I. Lee, K. S. Lee, J. H. Lee, I. S. Lee and S. H. Byeon, *Dalton Transactions*, 2009, 2490-2495.
30. Y. s. Yoon, B. I. Lee, K. S. Lee, G. H. Im, S. H. Byeon, J. H. Lee and I. S. Lee, *Advanced Functional Materials*, 2009, **19**, 3375-3380.
31. Y. Xu, A. Goyanes, Y. Wang, A. J. Weston, P. W. So, C. F. Gerald, A. M. Fogg, A. W. Basit and G. R. Williams, *Dalton Transactions*, 2018, **47**, 3166-3177.
32. M. Chen, H. M. Cooper, J. Z. Zhou, P. F. Bartlett and Z. P. Xu, *Journal of Colloid and Interface Science*, 2013, **390**, 275-281.
33. Y. Zhu, Z. Li, M. Chen, H. M. Cooper, G. Q. Lu and Z. P. Xu, *Chemistry of Materials*, 2012, **24**, 421-423.
34. X. Du, D. Zhang, R. Gao, L. Huang, L. Shi and J. Zhang, *Chemical Communications*, 2013, **49**, 6770-6772.
35. J. Liu, R. Harrison, J. Z. Zhou, T. T. Liu, C. Yu, G. Q. Lu, S. Z. Qiao and Z. P. Xu, *Journal of Materials Chemistry*, 2011, **21**, 10641.
36. L. Li, W. Gu, J. Liu, S. Yan and Z. P. Xu, *Nano Research*, 2015, **8**, 682-694.
37. T. Yokoi, Y. Sakamoto, O. Terasaki, Y. Kubota, T. Okubo and T. Tatsumi, *Journal of the American Chemical Society*, 2006, **128**, 13664-13665.
38. X. Du, D. Zhang, R. Gao, L. Huang, L. Shi and J. Zhang, *Chemical Communications*, 2013, **49**, 6770-6772.
39. F. Geng, Y. Matsushita, R. Ma, H. Xin, M. Tanaka, F. Izumi, N. Iyi and T. Sasaki, *Journal of the American Chemical Society*, 2008, **130**, 16344-16350.
40. C. Yu, H. Chu, Y. Wan and D. Zhao, *Journal of Materials Chemistry*, 2010, **20**, 4705-4714.
41. L. Li, G. Zi, W. Gu, L. Jian and P. X. Zhi, *Journal of Colloid & Interface Science*, 2016, **470**, 47-55.
42. C. R. Gordijo, C. A. S. Barbosa, A. M. D. C. Ferreira, V. R. L. Constantino and D. D. O. Silva, *Journal of Pharmaceutical Sciences*, 2010, **94**, -.
43. R. A. Rodríguez, C. Alvarez-Lorenzo and A. Concheiro, *European Journal of Pharmaceutical Sciences*, 2003, **20**, 429-438.
44. J. Wang, J. Zhou, Z. Li, Y. Song, Q. Liu, Z. Jiang and M. Zhang, *Chemistry - A European Journal*, 2011, **16**, 14404-14411.
45. G. Tuncelli, A. N. Ay and B. Zümreoglu-Karan, *Materials Science and Engineering C*, 2015, **55**, 562-568.
46. M. Rogosnitzky and S. Branch, *Biometals*, 2016, **29**, 365-376.
47. E. Rowatt and R. J. P. Williams, *Biochemical Journal*, 1989, **259**, 295-298.
48. H. Rohwer and E. Hosten, *Analytica Chimica Acta*, 1997, **339**, 271-277.

49. S. B. Savvin, *Talanta*, 1961, **8**, 673-685.
50. R. Borissova and E. Mitropolitska, *Talanta*, 1979, **26**, 543-547.
51. D. B. Gladilovich, V. Kubáň and L. Sommer, *Talanta*, 1988, **35**, 259-265.
52. M. Rabinovitch, *Trends in Cell Biology*, 1995, **5**, 85-87.
53. Z. Wolfgang, A. F. Neil and M.R. H. Adrian, *Journal of Controlled Release*, 2011, **71**, 39-51.
54. L. V. E. Juan, I. S. Igor, G. T. Brian and S. Y. L. Victor, *Small*, 2010, **6**, 1952-1967.
55. A. Prokop and J. M. Davidson, *Journal of Pharmaceutical Sciences*, 2008, **97**, 3518-3590.
56. Y. Zhu, J. Shi, W. Shen, X. Dong, J. Feng, M. Ruan and Y. Li, *Angewandte Chemie*, 2005, **117**, 5213-5217.
57. H. N. Wang, X. Meng, X. L. Wang, G. S. Yang and Z. M. Su, *Dalton Transactions*, 2012, **41**, 2231-2233.
58. M. S. Moorthy, J. H. Bae, M. J. Kim, S. H. Kim and C. S. Ha, *Particle and Particle Systems Characterization*, 2013, **30**, 1044-1055.59.
59. R. Bhaskar, R. Murthy, B. Miglani and K. Viswanathan, *International Journal of Pharmaceutics*, 1986, **28**, 59-66.
60. H. Zhang, D. Pan and X. Duan, *The Journal of Physical Chemistry C*, 2009, **113**, 12140-12148.
61. S. Hulbert, *Journal of the British Ceramic Society*, 1969, **6**, 11-20.
62. C. Markland, G. R. Williams and D. O'Hare, *Journal of Materials Chemistry*, 2011, **21**, 17896-17903.
63. J. Kim, Y. Piao and T. Hyeon, *Chemical Society Reviews*, 2009, **38**, 372-390.
64. Y. I. Park, J. H. Kim, K. T. Lee, K. S. Jeon, H. B. Na, J. H. Yu, H. M. Kim, N. Lee, S. H. Choi and S. I. Baik, *Advanced Materials*, 2009, **21**, 4467-4471.
65. J. Zhou, Y. Sun, X. Du, L. Xiong, H. Hu and F. Li, *Biomaterials*, 2010, **31**, 3287-3295.
66. R. Kumar, M. Nyk, T. Y. Ohulchanskyy, C. A. Flask and P. N. Prasad, *Advanced Functional Materials*, 2009, **19**, 853-859.
67. P. Caravan, J. J. Ellison, T. J. McMurry and R. B. Lauffer, *Chemical Reviews*, 1999, **99**, 2293-2352.
68. G. L. Davies, I. Kramberger and J. J. Davis, *Chemical Communications*, **49**, 9704-9721.
69. M. Wu, L. Li, X. Yu, D. Zhang, T. Sun, X. Li, L. Sun, S. Lui, X. Huang, B. Feng, H. Wang, H. Zhu and Q. Gong, *Journal of Biomedical Nanotechnology*, 2014, **10**, 3620-3630